Article

Effectively increased efficiency for electroreduction of carbon monoxide using supported polycrystalline copper powder electrocatalysts

Jing Li, Kuan Chang, Haochen Zhang, Ming He, William A. Goddard, Jingguang G Chen, Mu-Jeng Cheng, and Qi Lu

ACS Catal., **Just Accepted Manuscript** • Publication Date (Web): 18 Apr 2019

Effectively increased efficiency for electroreduction of carbon monoxide using supported polycrystalline copper powder electrocatalysts

Jing Li[1], Kuan Chang[1], Haochen Zhang[1], Ming He[1], William A. Goddard, III[2], Jingguang G. Chen[1,3], Mu-Jeng Cheng[4] & Qi Lu[1*]

[1]State Key Laboratory of Chemical Engineering, Department of Chemical Engineering, Tsinghua University, Beijing 100084, China.

[2]Materials and Process Simulation Center, California Institute of Technology, Pasadena, California 91125, United States.

[3]Department of Chemical Engineering, Columbia University, New York, New York 10027, United States.

[4]Department of Chemistry, National Cheng-Kung University, Tainan 701, Taiwan.

Jing Li and Kuan Chang contributed equally to this work.

*e-mail: luqicheme@mail.tsinghua.edu.cn

Abstract

Many electrocatalysts can efficiently convert CO_2 to CO. However, the further conversion of CO to higher-value products was currently hindered by the low activity of CO reduction reaction and the consequent lack of mechanistic insights for designing better catalysts. A flow-type reactor could potentially improve the reaction rate of CO reduction. However, the currently available configurations would pose great challenges in reaction mechanism understanding due to their complex nature and/or lack of precise potential control. Here we report, in standard electrochemical cell with three-electrode setup, a supported bulk polycrystalline copper powder electrode reduces CO to hydrocarbons and multi-carbon oxygenates with dramatically increased activities of more than 100 mA cm^{-2} and selectivities of more than 80%. The high activity and selectivity that was achieved demonstrates the practical feasibility of electrochemical CO or CO_2 (with a tandem strategy) conversion and enables the experimental exploration of the CO reduction mechanism to further reduced products.

Keywords: CO_2 reduction; CO reduction; copper; triple-phase-boundary; solar fuel; energy conversion.

Main

Electrochemical conversion of carbon dioxide (CO_2) into energy dense chemicals is an ideal technique for renewable energy storage and may potentially alleviate problems associated with CO_2 emissions.[1-5] Many electrocatalysts can efficiently reduce CO_2 to carbon monoxide (CO).[6-12] However, to achieve more valuable products, further reduction of CO is required. Copper (Cu) is the only known elemental electrocatalyst exhibiting appreciable activities toward such CO electroreduction.[13] Recent studies have shown that grain boundary terminated Cu surfaces are able to improve the selectivity and required energy bias for CO electroreduction.[14-15] Despite significant progress, the optimal activity achieved remains inadequate at less than 1 mA cm^{-2}, which is a factor of 100 too small for industrial application. This poor activity is attributed to the poor transport of CO due

to its low solubility in the electrolyte (ca. 1 mM). Moreover, the operational potential window for CO electroreduction is very small (ca. 0.2 V). At higher potentials, the competing hydrogen evolution reaction (HER) takes over the catalytic surface with a Faradaic efficiency of more than 80%.[14-15]

The problems associated with mass transport could potentially be reduced by introducing a flow-type reactor.[6, 16-18] However, this configuration poses great challenges when used for mechanistic investigations due to its highly custom-designed, complicated nature. For the same reason, although the membrane electrode assembly configuration for fuel cells have already been developed and commercialized for decades, electrode reaction studies (i.e., the hydrogen oxidation reaction and oxygen reduction reaction) and catalyst development are typically conducted using a batch-type 3-electrode setup. Moreover, at the current stage, the most commonly adapted flow-cell configurations for CO_2/CO electrolysis are not able to incorporate a reference electrode that is close enough to the working electrode.[6, 19] Therefore, a precise potential control is lacking and sometimes the electrode potential is only monitored through an external circuit.[6, 16, 20] High-rate flow-type electrodes can also be achieved by forcing the reactant gas stream onto the catalyst surface. However, it is difficult to establish a stable reaction interface in such configuration due to the vigorous physical contact of the gas bubbles to the catalyst surface.[21] Recently, the Kanan group reported a novel flow cell that included accurate potential control.[22] However, this configuration was designed for improving the single-pass conversion rate and is not suitable for probing reaction mechanism due to the reactant concentration can change drastically as it passes the patterned catalyst surface.

The insufficient understandings of reaction mechanisms underlying the electroreduction processes from CO_2 to CO and CO to hydrocarbons and oxygenates was one of the major obstacles in developing efficient electrocatalysts for achieving higher-value products.[23] For electroreduction of CO_2 in an aqueous electrolyte, the complex local pH environment influenced by the consumption of CO_2 and proton and their equilibria with bicarbonate posed great difficulties in mechanistic study, and sometimes led to controversial conclusions.[24-27] CO electroreduction is much more straightforward because CO does not participate in any electrolyte reactions. However, deep mechanistic investigations were hindered by the low activity and small operational potential window of previous catalysts.[28-30]

Herein, we report that a commercial bulk polycrystalline copper powder supported on carbon fiber paper electrode reduces CO to hydrocarbons and multi-carbon oxygenates with dramatically increased activities of more than 100 mA cm^{-2} and selectivities of more than 80% in a batch-type two-compartment electrochemical cell with a three-electrode setup (Figure S1). Isotope labeling studies confirm that the products are produced from reduction of CO in the electrolyte. This performance surpasses the performance of the best previously reported CO electroreduction catalysts by more than two orders of magnitude. The high activity and selectivity that was achieved demonstrates the practical feasibility of electrochemical CO or CO_2 (with a tandem strategy) conversion and greatly facilitates mechanistic analysis for deeper insight into these reactions. Our strategy may inspire the

catalyst development for electrolytic conversion processes of other low solubility gases, such as nitrogen and methane activation.

Results

CO electroreduction activity exceeding limiting value. The catalyst electrodes were prepared by depositing commercial polycrystalline Cu powders onto PTFE-treated carbon fiber paper (denoted as Cu/C) using protocols commonly employed for electrocatalysts that require a support.[6, 9, 31-32] Commercial Cu powders fabricated by either electrolysis in dendritic form from Sigma-Aldrich or atomization in spherical form from Alfa Aesar were used. Scanning electron microscopy (SEM) analysis indicated that both powders had sizes of several micrometers (Figure 1a-d). The powder X-ray diffraction patterns for both Cu powders exhibited peaks at the expected positions for an ideal Cu lattice (Figure e). Using the Scherrer method, we estimated the average crystallite size to be 54 nm for dendritic Cu and 50 nm for spherical Cu, indicating the polycrystalline nature of both Cu powders. A tiny peak associated with Cu_2O was observed for spherical Cu (at $2\theta = 36.48°$), and this peak may result from inevitable exposure to atmospheric air. The presence of Cu_xO was confirmed by X-ray photoelectron spectroscopy (XPS). This technique identified both Cu^{2+} and Cu^{+} on the surfaces of both Cu powders in addition to Cu^0 (Figure S2).

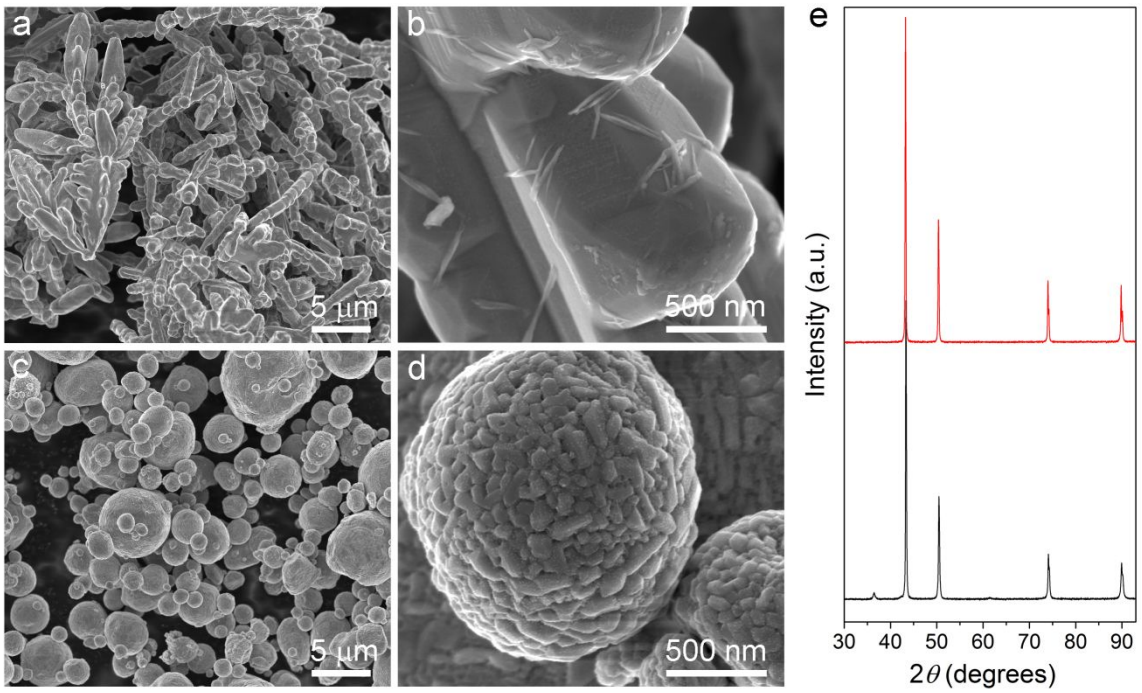

Figure 1. Physical characterization of Cu powders. a, b, SEM images of dendritic Cu powder from Sigma-Aldrich. **c, d,** SEM images of spherical Cu powder from Alfa Aesar. **e,** Powder X-ray diffraction patterns. Red line, dendritic Cu powder; blue line, spherical Cu powder.

CO electroreduction activity was measured under steady-state conditions by performing constant-potential electrolysis at ambient temperature. The electrolyte consisted of a 0.1 M KOH solution saturated with 1 atm of CO, leading to a concentration of approximately 1 mM. The gas-phase products were quantified using gas chromatography, and the liquid-phase products were quantified using nuclear magnetic resonance (NMR) spectroscopy. 2-hour electrolysis experiments were performed in an applied potential range (referenced to reversible hydrogen electrode (RHE) unless stated otherwise) of -0.50 V to approximately -0.94 V for dendritic Cu and to -0.89 V for spherical Cu (Figure S3 and S4). This potential window was selected to drive sufficient but not excessive reduction activities to establish reliable measurements. Very high CO electroreduction activities and selectivities were observed on both Cu powder electrodes (Figure 2). As the potential became more negative, the current density (referred to geometric current density unless stated otherwise) of dendritic Cu increased from approximately 1 mA cm^{-2} to near 180 mA cm^{-2}, and the Faradaic efficiency of the CO reduction increased from approximately 30% to more than 80% (Figure 2a, c). The current density behavior of spherical Cu was comparable to that of dendritic Cu. However, the highest Faradaic efficiency was ~70%, which was achieved at -0.78 V, but decreased slightly at more negative potentials (Figure 2b, d). The difference in product distribution of dendritic Cu and spherical Cu is likely due to their different surface conditions because they are fabricated using completely different techniques. These results are dramatically better than expected from the current understanding of the CO electroreduction reaction. Due to the low solubility of CO, the limiting current density of the CO electroreduction reaction for a planar electrode was estimated to be less than 1 mA cm^{-2} (see Methods), which was consistent with previously reported experimental results.[14-15, 21, 30, 33] In contrast, our Cu/C catalysts exhibit CO electroreduction current densities that exceed this limiting value by more than two orders of magnitude with no apparent transport limitations (Figure 1e, f).

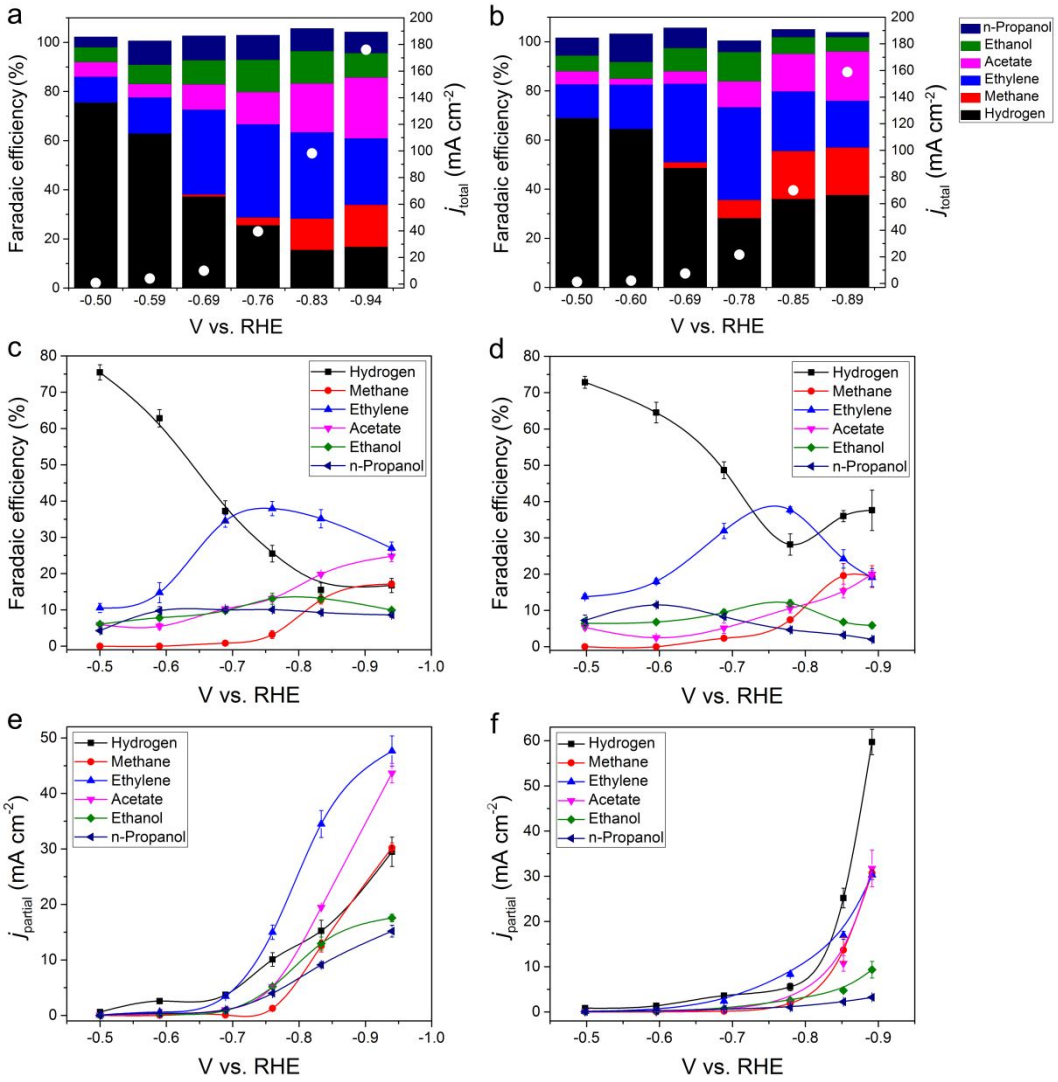

Figure 2. Electroreduction of CO by Cu/C catalysts in 0.1 M KOH saturated with 1 atm CO at ambient temperature. Left column, the dendritic Cu electrodes. Right column, the spherical Cu electrodes. **a, b,** total geometrical current densities and Faradaic efficiencies. **c, d,** Faradaic efficiencies and **e, f,** partial current densities for different reduction products. The error bar indicates the variation over 5 separate measurements using different electrodes.

Activity confirmed by isotope labeling experiment. An isotope labeling study using ^{13}CO confirmed that the high current densities resulted from the reduction of CO rather than other carbon sources (e.g., carbon support or organic contaminants) (Figure 3), and a controlled experiment using blank electrodes confirmed that the CO reduction activities were catalyzed by Cu powders (Figure S5). The mass spectroscopy data clearly showed the isotopic purity of the feeds during electrolysis using either ^{12}CO or ^{13}CO (Figure 3a). When replacing ^{12}CO with ^{13}CO, the parent ion of the produced ethylene shifted from m/z 28 to m/z 30 (Figure 3b) and that of methane shifted from m/z 16 to m/z 17 (Figure 3c), indicating the complete replacement of ^{12}C with ^{13}C in the gas-phase product. All the remaining ions in the mass fragmentation exhibited the expected shifts. For liquid products, the

^{1}H NMR spectra for acetate and ethanol exhibited the peak splitting expected for ^{13}C coupling when ^{13}CO was used (Figure 3d, e). The peaks associated with n-propanol were not evident after splitting due to its relatively low concentration. The very weak peaks associated with ^{12}C acetate and ethanol appeared in the ^{13}CO electrolysis spectra (less than 3% compared to their ^{13}C counterparts). This result was most likely due to the existence of $K_2{}^{12}CO_3$ (byproduct of KOH manufacturing) in the KOH electrolyte, which could provide a ^{12}C source, such as $^{12}CO_2$ and $H^{12}CO_3^-$, via aqueous equilibria.

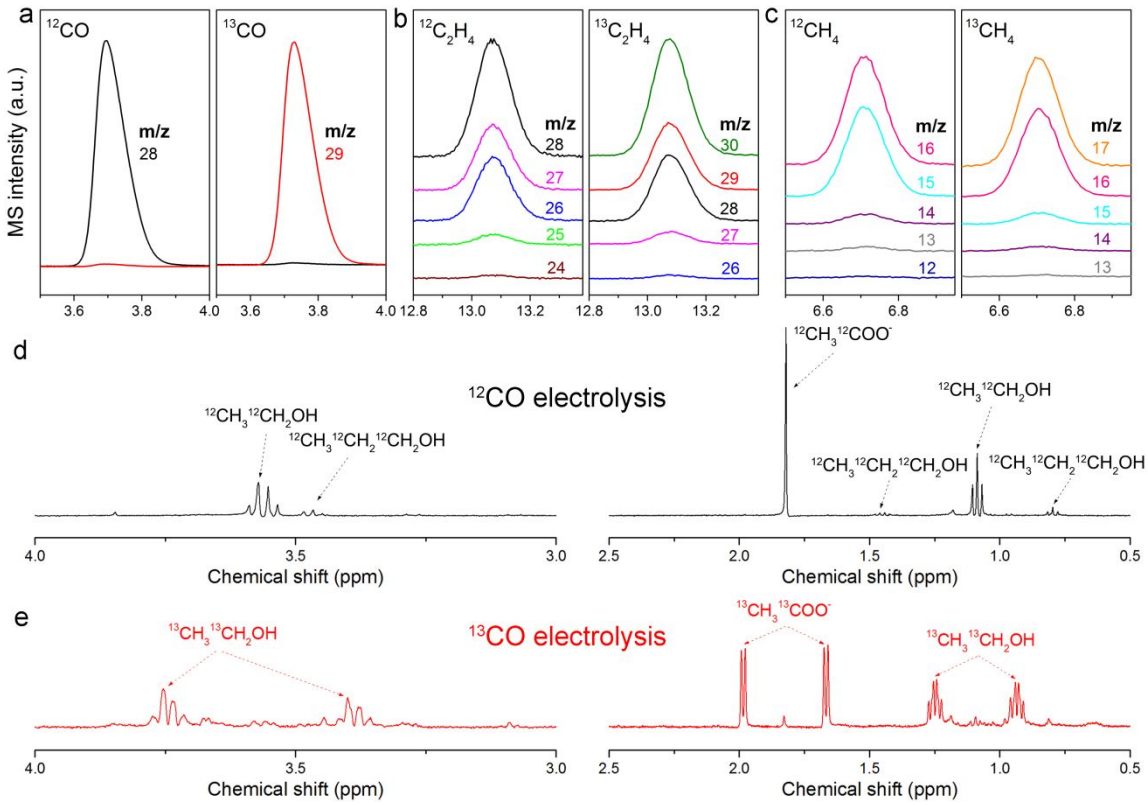

Figure 3. Isotope labeling study. Mass fragmentation patterns CO (a), ethylene (b) and methane (c). ^{1}H NMR spectra of the electrolyte after ^{12}CO (d) and ^{13}CO (e) electrolysis.

Probing the origins of the high activity. To investigate the origins of the high CO electroreduction activity of the Cu/C catalysts, we first considered that the improvement in the limiting current may be due to unusually active sites on the Cu powder surface, which were able to interact with dissolved CO molecules in a way that decreased its hydrodynamic boundary layer thickness.[21, 34] To verify this hypothesis, we annealed the dendritic Cu under 5% H_2 in Ar at elevated temperatures of 300 and 500 °C, which was sufficient to relax its microstructure and flatten its surface.[15, 35] However, the annealed dendritic Cu exhibited no obvious performance changes compared to its pristine counterpart (Figure S6), indicating that the surface conditions were not key in achieving the extremely high CO reduction activity. The electrochemical active surface area (ECSA) of dendritic Cu/C electrode was determined to be 0.5 $cm^2{}_{ECSA}$ /$cm^2{}_{geo}$ using the underpotential deposition (UPD) of lead method (Figure S7), which indicates that the ECSA or roughness factor is not responsible to this high rate either.

Next, we considered possible enhancement of CO transport due to the formation of triple-phase-boundaries at the catalyst-support interfaces. Due to the hydrophobic nature of the carbon fiber paper surface, the electrolyte may not be able to wet the interface area, which would leave gas-phase spaces filled with CO molecules through exchange with the CO saturated electrolyte. In this scenario, the catalyst surface, electrolyte, and CO gas would come into direct contact at their common boundaries such that CO electroreduction would no longer be limited by the low solubility of CO in the electrolyte. To verify this hypothesis, we compared the performance of a free-standing Cu wire with an electrode prepared by attaching the Cu wire onto a carbon fiber paper support (Figure S8). While the performance of the free-standing Cu wire should be limited by CO transport as conventional electrodes, this same material should exhibit a drastically enhanced performance if the triple-phase-boundaries are formed when supported on the hydrophobic carbon fiber paper. The free-standing Cu wire primarily produced H_2 with a Faradaic efficiency for the CO electroreduction of only approximately 10%, which is consistent with results obtained on a polycrystalline Cu foil at the same potential.[15, 30] However, the supported Cu wire electrode exhibited a significant improvement in the CO electroreduction selectivity to more than 50%. We performed additional controlled experiments to exclude the possibilities that the reactant CO was transported from the top part of the carbon paper or through the physical contact of purging gas (Figures S9 and S10). These experimental results clearly demonstrate that the tremendous enhancement of the CO electroreduction results from establishing an interface between the Cu surface and the carbon fiber paper, overcoming the limitations associated with the low solubility of CO in the electrolyte. The hydrophobicity of the catalyst support is key in forming triple-phase-boundaries and achieving high reaction rates. The dendritic Cu powders deposited on non-hydrophobic carbon support (i.e., non-PTFE-treated carbon fiber paper and glassy carbon) did not show the merit in improving the performance of CO electroreduction (Figure S11). The CO transport of our electrode versus conventional electrodes is described in Scheme 1. We also propose that the morphology of Cu catalysts may affect the nature of triple-phase-boundaries (e.g. size and geometry), which can be a plausible cause to the different product distribution for dendritic Cu and spherical Cu (Figure 2).

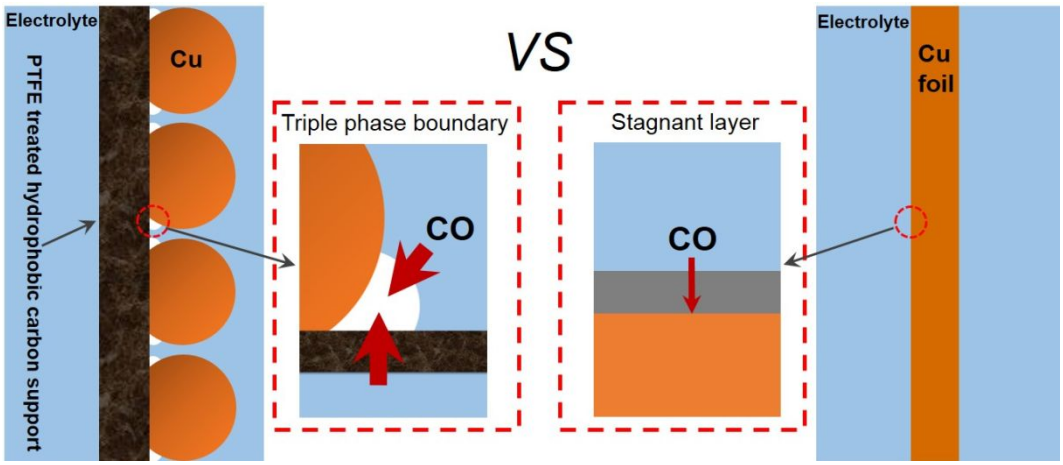

Scheme 1. **CO mass transport.** The Cu/C electrode vs. conventional electrode.

This hydrophobic catalyst-support interface did not improve CO_2 electroreduction. This result was expected because carbon fiber paper supports are widely used in CO_2 electrolysis with no additional improvements.[31, 36-38] When we used the same Cu powder electrodes for CO_2 electroreduction, the obtained performance was similar to that of bulk Cu foils (Figure S12).[39-40] We believe that this result was due to the increase in the pH near the electrode surface, resulting from generation of OH^- and CO_3^{2-} during CO_2 electrolysis[13, 24] that prevented CO_2 from passing through to contact the Cu surface as gas-phase molecules.

Enabling experimental probing for deeper mechanistic insights. For electroreduction of CO_2 in an aqueous electrolyte, the local pH increase diminishes the CO_2 concentration at the electrode surface and decreases the rate of CO_2 replenishment from the CO_2/bicarbonate equilibrium, posing great complications in understanding the mechanisms underlying the reduction processes from CO_2 to CO and CO to hydrocarbons and oxygenates.[25, 27] Although CO electroreduction is much more straightforward because CO does not participate in any electrolyte reactions, mechanistic studies are hindered by the low activity and small operational potential window of previous catalysts.[14, 35, 41] Due to its significantly improved efficiency, our Cu/C catalysts enabled mechanistic probing for deeper insight into the conversion of CO to further reduced products.

Figure 4a-d showed the linear Tafel curves for all CO electroreduction products obtained on dendritic Cu/C electrodes excluding the transport-limited data points at most negative potential of -0.94 V. All C_{2+} products exhibited a similar Tafel slope of approximately 120-140 mV dec^{-1}, implying that they share the same rate-determining step (RDS) which involves an initial one-electron transfer.[36, 42-44] However, CH_4 exhibited a Tafel slope of approximately 60 mV dec^{-1}, implying that its RDS is a chemical step after a pre-equilibrium one-electron transfer.[36, 42-44] To obtain more information of reaction kinetics, CO partial pressure dependence study was conducted at a constant potential, and the results were shown in Figure 4e, f. The partial current density for all C_{2+} products formation increased steadily as the CO partial pressure increased from 0.05 to 0.6 atm. However, as the CO partial pressure increased from 0.6 to 1.0 atm, the formation rates of all CO reduction products ceased to increase with respect to the CO concentration in electrolyte. This indicates that the catalyst surface is saturated with CO and the reduction reaction is entirely limited by kinetics (Figure 4e, f). Interestingly, the CH_4 production rate behaved very differently than the C_{2+} products. The CH_4 partial current density decreased as the CO partial pressures were further increased from 0.2 atm (Figure 4e). This suggests that a change in the CO concentration may affect intermediates other than *CO in the rate-determining step (RDS) for CH_4 formation.

According to the current understanding, the RDS of CH_4 formation involves protonation of *CO to *CO(H) (i.e., hydrogenated *CO). However, the proton source (i.e., surface-adsorbed *H, H^+, or H_2O) remains unclear. The RDS of C_{2+} products formation is much more ambiguous. Many possible RDSs have been proposed by various research groups and can be summarized as follows: (1) dimerization of 2 surface-adsorbed *CO,[45-47] (2) dimerization of 1 surface-adsorbed *CO with 1 unabsorbed CO molecule,[48] and (3) protonation of *CO to

*CO(H) followed by fast coupling with *CO (or CO molecule) to form the C-C bond.[49-50] We calculated the Tafel slopes and reaction orders of CH_4 and C_{2+} products formation with respect to the CO concentration by considering these possible RDSs, as described in the Supplementary Methods. As a result, the negative reaction order of CH_4 formation as well as its Tafel slope being close to 59 mV dec^{-1} indicate that the RDS involves *CO protonation with the proton sources being surface-adsorbed *H (Table S1). This result is due to *H being the only proton source whose availability can decrease due to an increase in surface-adsorbed *CO, which is evident as the H_2 production rate was consistently decreased as the increase of CO partial pressure (Figure 4e). The zero-order dependence of C_{2+} products formation as well as their Tafel slopes being close to 118 mV dec^{-1} indicate that the RDS is the dimerization of 2 surface-adsorbed *CO (Table S2). The proposed RDS (2) would generate a reaction order of 1 at high CO coverage which is inconsistent with our experimental observation. The proposed RDS (3) can also be consistent with the obtained reaction kinetics if the proton source is H^+ or H_2O (Table S2). However, such reaction scheme would lead to a pH dependence of C_{2+} products formation which is apparently against the current understanding that the C_2H_4 formation is pH independent.[28, 34, 51-52] Based on these mechanistic analyses, the RDSs of CO electroreduction reaction can now be summarized in Figure 4g. This is the first time that such kinetic insights were experimentally determined in the system that is mostly desired for carrying out this reaction (i.e., aqueous electrolyte and ambient conditions). These RDSs are also consistent with the recently proposed microkinetic model based on density functional theory computations.[53]

It is worth noting however, that ideally, the Tafel slope is an inherent property of electrocatalytic materials and is a useful indicator of the rate-limiting step for reactions involving electron transfer. In reality, the Tafel slope can be dependent on many factors other than the kinetic exponent of the electrons, such as the presence of adsorbates and the mass transport effect. The high reaction rate of our electrode may accumulate excess products near electrode surface that may affect Tafel analysis and the high CO mass transport scheme may complex the current kinetic models. More systematic studies using different electrolyte pH, cations, and concentrations are highly desired future works for providing a more complete picture of CO_2/CO electroreduction reaction.

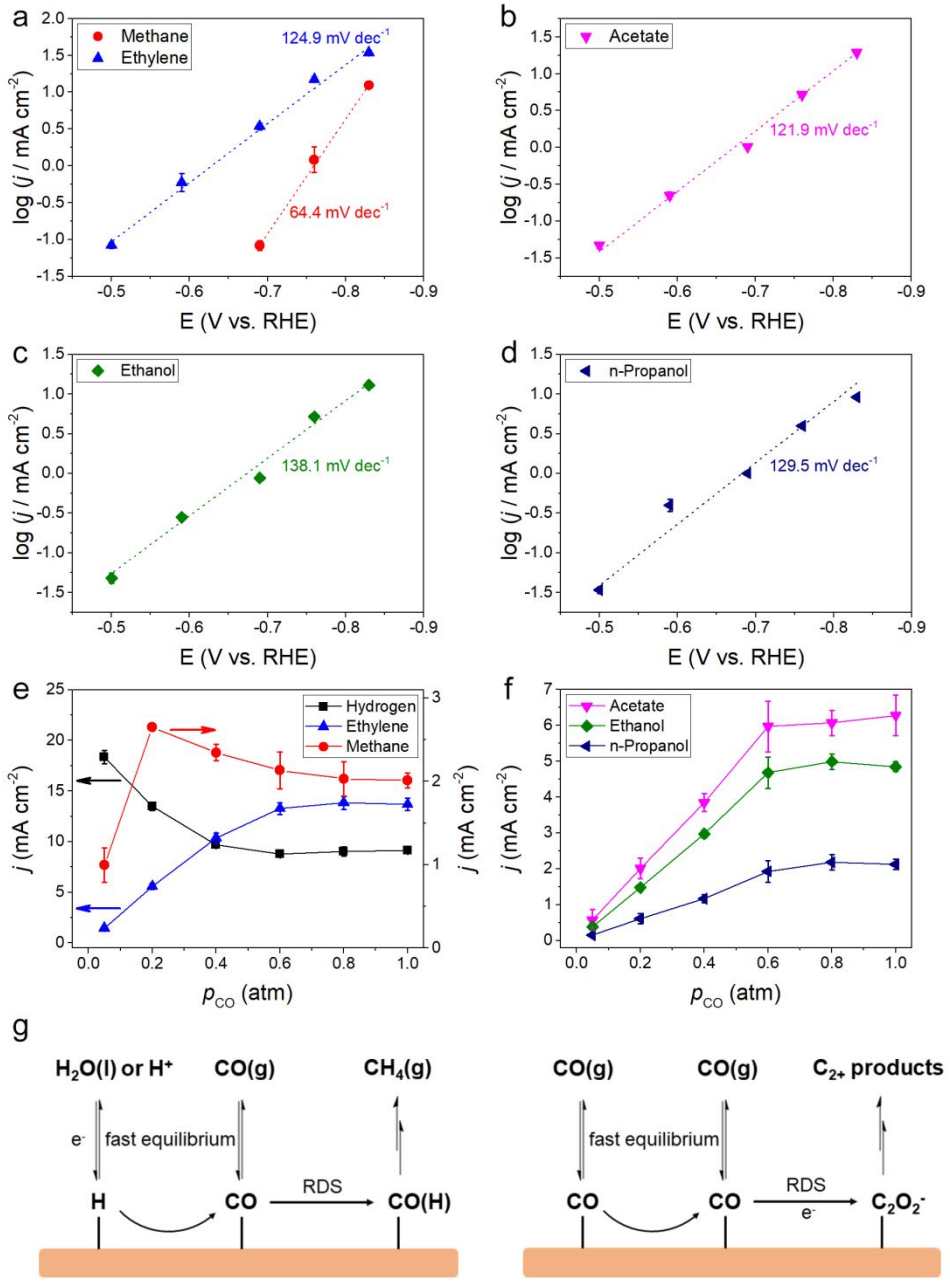

Figure 4. Mechanism study. Tafel analysis for methane and ethylene (a), acetate (b), ethanol (c) and n-propanol (d) production. Partial current densities for gas products (e) and liquid products (f) versus CO partial pressure at -0.78 V. Schematics of RDS for CH_4 and C_{2+} products formation (g). The error bar indicates the standard deviation of partial current densities over 5 separate experimental measurements using different samples.

Conclusion

The studied Cu/C catalysts look very promising for the efficient synthesis of value-added chemicals via the electroreduction of CO or CO_2 (perhaps using a tandem strategy) powered by renewable energy. By eliminating the limitation of low CO solubility in the electrolyte, we achieved very high current density (more than 100 mA

cm^{-2}), which meets the standard for industrial electrolyzers. The experimental investigations for reliable mechanistic understanding of CO and CO_2 electroreduction were greatly facilitated. In addition, our strategy employs a gas diffusion mechanism that is the essence of flow-cell configurations. Therefore, the catalysts explored using our strategy can be transferred to flow-cell configurations to significantly reduce the gap between basic and applied research, which is currently a serious problem in the development of fuel cell catalysts due to the intrinsic difference between rotating disk electrode and flow-cell configurations. Moreover, our strategy may inspire the development of new generation catalysts for electrolytic conversion of other gases with low solubility, such as nitrogen and methane. With such high rates, the experimental exploration of the CO reduction mechanism to further reduced products will be accessible.

Methods

Materials. Potassium hydroxide (semiconductor grade, 99.99% trace metals basis) was purchased from Sigma-Aldrich. Potassium carbonate (99.997% trace metals basis) was purchased from Alfa Aesar. Chelex 100 sodium form was purchased from Sigma-Aldrich. Perchloric acid (99.999% trace metal basis) was purchased from Sigma-Aldrich. Lead(II) perchlorate trihydrate (97% ACS grade) was purchased from Alfa Aesar. Carbon monoxide (99.999%), argon (99.999%) and 5% hydrogen in argon gases were purchased from Air Liquide. ^{13}C-labeled carbon monoxide (isotopic enrichment ≥ 99%) was purchased from Linde. Cu powder in dendritic form (<45 μm, 99.7% trace metals basis) was purchased from Sigma-Aldrich, and Cu powder in spherical form (-625 mesh, 99.9% metals basis) was purchased from Alfa Aesar. Cu wire (0.127 mm dia, 99.999% metals basis) was purchased from Alfa Aesar. Cu foil (0.1mm thick, 99.9999% metal basis) was purchased from Alfa Aesar. The carbon fiber paper support (Sigracet 29 BC (with PTFE treatment) and Sigracet 29 AA (no PTFE treatment)) was purchased from the Fuel Cell Store. The glassy carbon support (type 2) was purchased from Alfa Aesar. Nafion solution (5 wt %) was purchased from Sigma-Aldrich. The electrolyte solutions were prepared using Milli-Q water (18.2 MΩ cm).

Physical Characterizations. The field emission scanning electron microscope images were recorded on a Merlin FE-SEM from Zeiss. Powder X-ray diffraction patterns were obtained using a Rigaku MiniFlex 600 with Cu Kα radiation. X-ray photoelectron spectroscopy measurements were carried out using a PHI Quantera II. The resulting spectra were analyzed using the CasaXPS software package (Casa Software Ltd., U.K.).

Electrode preparation. To prepare the polycrystalline Cu powder electrodes, 8 mg of Cu powder were uniformly dispersed onto an 8 cm^2 Sigracet 29 BC or Sigraect 29 AA carbon fiber paper to achieve a catalyst loading of approximately 1.0 mg cm^{-2}. Next, 200 μL of a 2.5 wt % Nafion solution were uniformly deposited onto the catalyst layer. After drying in air, the catalyst was further dried under vacuum to thoroughly remove the residual solvent. Then, the catalyst was cut into individual electrodes that were approximately 0.5 × 1.5 cm. A nickel wire current collector was subsequently attached to one end of the electrode using silver epoxy. The blank electrodes for the controlled experiment were prepared using identical procedures except for the introduction of the Cu powder.

The glassy carbon supported Cu electrodes were prepared using glassy carbon plates cut to a size of approximately 0.5 × 2 cm. The mass of Cu powder and the volume of Nafion solution used for deposition were adjusted to achieve the same mass loading of 1.0 mg cm^{-2}. The annealed Cu powder electrodes were prepared using dendritic Cu powders that were annealed under 5% H_2 in Ar at the desired temperatures for 2 hours using a tube furnace. The free-standing Cu wire electrode consisted of a Cu wire after electrochemical polishing. The supported Cu wire electrode was prepared by cutting an electrochemically polished Cu wire into millimeter-long pieces followed by deposition onto a carbon fiber paper using the same method as that employed to prepare the Cu powder electrodes.

Electrochemical measurements. A Gamry Reference 600+ Potentiostat was used for all electrochemical measurements. A graphite rod (Sigma-Aldrich, 99.999%) was used as the counter electrode. The electrolyte used for all CO electroreduction consisted of a 1 atm CO-saturated 0.1 M KOH solution with a pH of 13. The electrolysis potential was measured against a Hg/HgO reference electrode (1.0 M KOH), which was calibrated using a homemade standard hydrogen electrode. The electrolyte used for all CO_2 electroreductions consisted of 0.1 M CO_2-saturated $KHCO_3$ with a pH of 6.8. The $KHCO_3$ solution was prepared by dissolving K_2CO_3 in Milli-Q water (18.2 MΩ cm) followed by purging with high purity CO_2 gas (99.999%, Air Liquide) for at least 10 hours. The electrolyte was purified using Chelex prior to electrolysis. An Ag/AgCl (3.0 M KCl, BASi) electrode was used as the reference electrode. The measured potential was converted to the RHE reference scale as follows:

$$\text{Potential (vs. RHE)} = \text{Potential (vs. Hg/HgO)} + 0.140\ \text{V} + 0.0591\ \text{V} \times \text{pH}$$

$$\text{Potential (vs. RHE)} = \text{Potential (vs. Ag/AgCl)} + 0.210\ \text{V} + 0.0591\ \text{V} \times \text{pH}$$

The uncompensated resistance (R_u) was determined by potentiostatic electrochemical impedance spectroscopy. The potentiostat compensated for 85% of R_u during the electrolysis, and the remaining 15% was manually corrected afterwards to arrive at the actual potentials.

Electroreduction evaluation. A custom designed gas-tight two-compartment electrochemical cell fabricated by Adams & Chittenden Scientific Glass was used for all electrolysis experiments. The cell was sonicated in a mixture of nitric acid and hydrochloric acid and thoroughly cleaned with Milli-Q water prior to electrolysis. The two compartment chambers were separated by a piece of anion-conducting membrane (Selemion AMV AGC Inc.). The electrolyte in the cathode chamber was 18.0 ml leaving a headspace volume of 15.8 ml. CO or CO_2 gas was delivered into the electrolyte through a gas dispersion frit to ensure sufficient gas-electrolyte mixing at a flow rate of 10.00 cm^3 min^{-1}. The flow rate was controlled by a mass flow controller (MKS Instruments Inc.) and calibrated using an ADM flow meter from Agilent Technologies. The headspace gas was vented directly into the sampling loop of a gas chromatograph (Agilent 7890B) and quantified every 17 mins for gas-phase products. The gas chromatograph was equipped with a ShinCarbon ST column and a HayeSep Q column. Argon (Air Liquide, 99.999%) was used as the carrier gas. A flame ionization detector with a methanizer was used to quantify C_2H_4

and CH_4. A thermal conductivity detector was used to quantify the H_2 concentration. The liquid-phase products were quantified on a Bruker AVIII 400 MHz NMR spectrometer. The NMR sample was prepared by mixing 500 μL of the electrolyte with 100 μL of D_2O (Sigma-Aldrich, 99.9%) and 1.67 p.p.m. (m/m) dimethyl sulfoxide (Alfa Aesar, ≥99.9%) as an internal standard. The water signal was suppressed using the presaturation method.

Activity vs. potential plots. Each data point in the Faraday efficiency and partial current density as a function of potential plots was obtained in an individual electrolysis experiment using a freshly prepared electrode. All electrodes were pretreated at –1.0 V for 5 mins in the argon-purged electrolyte to stabilize the surface conditions prior to the CO electroreduction measurements. The electrolysis time was more than 2 hours during which 8 periodical gas chromatograph analyses were performed, and the results were averaged. The liquid products were analyzed at the conclusion of the electrolysis. In the partial pressure dependence plots, the CO partial pressures, which ranged from 0.05 to 1.0 atm, were achieved by mixing CO and argon gases at the desired ratio using mass flow controllers after calibration. One single dendritic Cu/C electrode was used for the CO partial pressure dependence study to eliminate the variations between the different electrodes. A 10 min electrolysis was conducted at each CO concentration. Then, the reaction products were sampled for the measurement, and the electrolysis was performed on the next CO concentration. The total electrolysis time for the CO partial pressure dependence study was less than 2 hours, in which the dendritic Cu/C electrode was stable to generate reliable data for analysis (Figure S3).

Isotopic labeling study. In ^{13}CO electrolysis, ^{13}CO was not continuously delivered into the cathode chamber as in ^{12}CO electrolysis. The electrochemical cell was completely sealed after both the electrolyte and headspace were purged with ^{13}CO at 50.00 cm^3 min^{-1} for 5 mins. The electrolysis was performed using a dendritic Cu/C electrode at -0.74 V for 2 hours. The gas-phase products were sampled using a gas-tight syringe (Hamilton) and analyzed using a homebuilt gas chromatograph (Agilent 7890B) – mass spectroscopy (Hiden HPR-40) system. The liquid-phase products were analyzed in the same way as in ^{12}CO electrolysis.

Limiting current density estimation. Fick's law of diffusion (equation (1)) was used to estimate the limiting current density for a planar electrode in the electroreduction of CO. j is the CO electroreduction current density. D_0 is the diffusion coefficient ($D_0 = 2.1 \times 10^{-9}$ m^2 s^{-1} at 20 °C). C_0 is the solubility of CO in an aqueous solution ($C_0 = 1$ mM at 20 °C). n is the number of electrons involved in the reaction, which was chosen to be 4 by assuming that the composition of the reaction products consisted of 35% ethylene, 10% ethanol, 5% n-propanol, 25% methane, and 25% acetate. L is the hydrodynamic boundary layer thickness, which was approximately 100 μm under moderate stirring/convection conditions in the literature.[21] F is the Faraday constant. If only one side of the planar electrode participates in the electroreduction, the limiting current density due to mass transport was calculated to be approximately 0.8 mA cm^{-2}. If the electrodes possess 3-D geometry or multiple sides participate in the reaction, the mass transport-limited current density can be higher than the calculated value.

$$j = nFD_0 \frac{C_0}{L} \quad (1)$$

Electrochemically active surface area measurement. The ECSAs of the dendritic Cu/C electrodes were measured using Pb underpotential deposition in a degassed solution that consisted of 0.1 M $HClO_4$ and 0.001 M $Pb(ClO_4)_2$ in an Ar atmosphere.[54-56] The Pb underpotential deposition was carried out using cyclic voltammetry. The potential window ranged from -450 mV to -100 mV vs. Ag/AgCl (3 M KCl), and the scanning rates were 10, 20, 50, 80, and 100 mV s^{-1}. The integration of the Pb stripping current peak between -350 mV and -200 mV vs. Ag/AgCl was plotted as a function of the scanning rate. The slope of the linear regression yields the charge for the oxidation of a monolayer of Pb adatoms over Cu. Then, the charge was divided by 329.3 μC cm^{-2}_{ECSA}, which was obtained from an electropolished Cu foil and consistent with the literature[54], to estimate the actually surface area of dendritic Cu/C electrodes that can be accessed by the electrolyte.

Acknowledgements

This work was supported by the National Basic Research of China (grant number 2017YFA0208200) and the National Natural Science Foundation of China (grant number 21872079, 21606142). M.J.C. acknowledges financial support from the Ministry of Science and Technology of the Republic of China under grant no. MOST 107-2113-M-006-008-MY2.

Supporting Information

Image of the electrochemical H-cell, XPS characterizations, chronoamperometry profiles, ECSA measurements, controlled experiments, CO_2 electrolysis results, and predictions of Tafel slope and reaction order for possible rate determining steps.

Reference

1. Costentin, C.; Robert, M.; Saveant, J. M. Catalysis of the Electrochemical Reduction of Carbon Dioxide. *Chem. Soc. Rev.* **2013,** 42, 2423-2436.
2. Wang, W. H.; Himeda, Y.; Muckerman, J. T.; Manbeck, G. F.; Fujita, E. CO2 Hydrogenation to Formate and Methanol as an Alternative to Photo- and Electrochemical CO2 Reduction. *Chem. Rev.* **2015,** 115, 12936-12973.
3. Lewis, N. S. Research Opportunities to Advance Solar Energy Utilization. *Science* **2016,** 351.
4. Chu, S.; Cui, Y.; Liu, N. The Path Towards Sustainable Energy. *Nat. Mater.* **2017,** 16, 16-22.
5. Montoya, J. H.; Seitz, L. C.; Chakthranont, P.; Vojvodic, A.; Jaramillo, T. F.; Norskov, J. K. Materials for Solar Fuels and Chemicals. *Nat. Mater.* **2017,** 16, 70-81.
6. Rosen, B. A.; Salehi-Khojin, A.; Thorson, M. R.; Zhu, W.; Whipple, D. T.; Kenis, P. J. A.; Masel, R. I. Ionic Liquid-Mediated Selective Conversion of CO2 to CO at Low Overpotentials. *Science* **2011,** 334, 643-644.
7. Zhu, W. L.; Michalsky, R.; Metin, O.; Lv, H. F.; Guo, S. J.; Wright, C. J.; Sun, X. L.; Peterson, A. A.; Sun, S. H. Monodisperse Au Nanoparticles for Selective Electrocatalytic Reduction of CO2 to CO. *J. Am. Chem. Soc.* **2013,** 135, 16833-16836.

8. Asadi, M.; Kumar, B.; Behranginia, A.; Rosen, B. A.; Baskin, A.; Repnin, N.; Pisasale, D.; Phillips, P.; Zhu, W.; Haasch, R.; Klie, R. F.; Kral, P.; Abiade, J.; Salehi-Khojin, A. Robust Carbon Dioxide Reduction on Molybdenum Disulphide Edges. *Nat. Commun.* **2014,** 5, 4470.
9. Lu, Q.; Rosen, J.; Zhou, Y.; Hutchings, G. S.; Kimmel, Y. C.; Chen, J. G. G.; Jiao, F. A Selective and Efficient Electrocatalyst for Carbon Dioxide Reduction. *Nat. Commun.* **2014,** 5, 3242.
10. Medina-Ramos, J.; DiMeglio, J. L.; Rosenthal, J. Efficient Reduction of CO2 to CO with High Current Density Using in Situ or Ex Situ Prepared Bi-Based Materials. *J. Am. Chem. Soc.* **2014,** 136, 8361-8367.
11. Hall, A. S.; Yoon, Y.; Wuttig, A.; Surendranath, Y. Mesostructure-Induced Selectivity in CO2 Reduction Catalysis. *J. Am. Chem. Soc.* **2015,** 137, 14834-14837.
12. Liu, M.; Pang, Y. J.; Zhang, B.; De Luna, P.; Voznyy, O.; Xu, J. X.; Zheng, X. L.; Dinh, C. T.; Fan, F. J.; Cao, C. H.; de Arquer, F. P. G.; Safaei, T. S.; Mepham, A.; Klinkova, A.; Kumacheva, E.; Filleter, T.; Sinton, D.; Kelley, S. O.; Sargent, E. H. Enhanced Electrocatalytic CO2 Reduction Via Field-Induced Reagent Concentration. *Nature* **2016,** 537, 382-386.
13. Hori, Y. Electrochemical CO2 Reduction on Metal Electrodes. *Mod. Aspects Electrochem.* **2008**, 42, 89-189.
14. Li, C. W.; Ciston, J.; Kanan, M. W. Electroreduction of Carbon Monoxide to Liquid Fuel on Oxide-Derived Nanocrystalline Copper. *Nature* **2014,** 508, 504-507.
15. Verdaguer-Casadevall, A.; Li, C. W.; Johansson, T. P.; Scott, S. B.; McKeown, J. T.; Kumar, M.; Stephens, I. E. L.; Kanan, M. W.; Chorkendorff, I. Probing the Active Surface Sites for CO Reduction on Oxide-Derived Copper Electrocatalysts. *J. Am. Chem. Soc.* **2015,** 137, 9808-9811.
16. Ma, S. C.; Sadakiyo, M.; Luo, R.; Heima, M.; Yamauchi, M.; Kenis, P. J. A. One-Step Electrosynthesis of Ethylene and Ethanol from CO2 in an Alkaline Electrolyzer. *J. Power Sources* **2016,** 301, 219-228.
17. Dinh, C. T.; Burdyny, T.; Kibria, M. G.; Seifitokaldani, A.; Gabardo, C. M.; de Arquer, F. P. G.; Kiani, A.; Edwards, J. P.; De Luna, P.; Bushuyev, O. S.; Zou, C. Q.; Quintero-Bermudez, R.; Pang, Y. J.; Sinton, D.; Sargent, E. H. CO2 Electroreduction to Ethylene Via Hydroxide-Mediated Copper Catalysis at an Abrupt Interface. *Science* **2018,** 360, 783-787.
18. Zhuang, T. T.; Liang, Z. Q.; Seifitokaldani, A.; Li, Y.; De Luna, P.; Burdyny, T.; Che, F. L.; Meng, F.; Min, Y. M.; Quintero-Bermudez, R.; Dinh, C. T.; Pang, Y. J.; Zhong, M.; Zhang, B.; Li, J.; Chen, P. N.; Liang, H. Y.; Ge, W. N.; Ye, B. J.; Sinton, D.; Yu, S. H.; Sargent, E. H. Steering Post-C-C Coupling Selectivity Enables High Efficiency Electroreduction of Carbon Dioxide to Multi-Carbon Alcohols. *Nat. Catal.* **2018,** 1, 421-428.
19. Jouny, M.; Luc, W.; Jiao, F. High-Rate Electroreduction of Carbon Monoxide to Multi-Carbon Products. *Nat. Catal.* **2018,** 1, 748-755.
20. Hoang, T. T. H.; Verma, S.; Ma, S. C.; Fister, T. T.; Timoshenko, J.; Frenkel, A. I.; Kenis, P. J. A.; Gewirth, A. A. Nanoporous Copper Silver Alloys by Additive-Controlled Electrodeposition for the Selective Electroreduction of CO2 to Ethylene and Ethanol. *J. Am. Chem. Soc.* **2018,** 140, 5791-5797.
21. Han, L. H.; Zhou, W.; Xiang, C. X. High-Rate Electrochemical Reduction of Carbon Monoxide to Ethylene Using Cu-Nanoparticle-Based Gas Diffusion Electrodes. *ACS Energy Lett.* **2018,** 3, 855-860.
22. Ripatti, D. S.; Veltman, T. R.; Kanan, M. W. Carbon Monoxide Gas Diffusion Electrolysis That Produces Concentrated C2 Products with High Single-Pass Conversion. *Joule* **2019,** 3, 240-256.
23. Seh, Z. W.; Kibsgaard, J.; Dickens, C. F.; Chorkendorff, I. B.; Norskov, J. K.; Jaramillo, T. F. Combining Theory and Experiment in Electrocatalysis: Insights into Materials Design. *Science* **2017,** 355.
24. Singh, M. R.; Kwon, Y.; Lum, Y.; Ager, J. W.; Bell, A. T. Hydrolysis of Electrolyte Cations Enhances the Electrochemical Reduction of CO2 over Ag and Cu. *J. Am. Chem. Soc.* **2016,** 138, 13006-13012.
25. Dunwell, M.; Lu, Q.; Heyes, J. M.; Rosen, J.; Chen, J. G. G.; Yan, Y. S.; Jiao, F.; Xu, B. J. The Central Role of Bicarbonate in the Electrochemical Reduction of Carbon Dioxide on Gold. *J. Am. Chem. Soc.* **2017,** 139, 3774-3783.
26. Perez-Gallent, E.; Marcandalli, G.; Figueiredo, M. C.; Calle-Vallejo, F.; Koper, M. T. M. Structure- and Potential-Dependent Cation Effects on CO Reduction at Copper Single-Crystal Electrodes. *J. Am. Chem. Soc.* **2017,** 139, 16412-16419.
27. Wuttig, A.; Yoon, Y.; Ryu, J.; Surendranath, Y. Bicarbonate Is Not a General Acid in Au-Catalyzed CO2 Electroreduction. *J. Am. Chem. Soc.* **2017,** 139, 17109-17113.

28. Schouten, K. J. P.; Qin, Z. S.; Gallent, E. P.; Koper, M. T. M. Two Pathways for the Formation of Ethylene in CO Reduction on Single-Crystal Copper Electrodes. *J. Am. Chem. Soc.* **2012,** 134, 9864-9867.
29. Roberts, F. S.; Kuhl, K. P.; Nilsson, A. Electroreduction of Carbon Monoxide over a Copper Nanocube Catalyst: Surface Structure and pH Dependence on Selectivity. *Chemcatchem* **2016,** 8, 1119-1124.
30. Bertheussen, E.; Hogg, T. V.; Abghoui, Y.; Engstfeld, A. K.; Chorkendorff, I.; Stephens, I. E. L. Electroreduction of CO on Polycrystalline Copper at Low Overpotentials. *ACS Energy Lett.* **2018,** 3, 634-640.
31. Kim, D.; Kley, C. S.; Li, Y. F.; Yang, P. D. Copper Nanoparticle Ensembles for Selective Electroreduction of CO2 to C2-C3 Products. *Proc. Natl. Acad. Sci. U. S. A.* **2017,** 114, 10560-10565.
32. Ma, S.; Sadakiyo, M.; Heima, M.; Luo, R.; Haasch, R. T.; Gold, J. I.; Yamauchi, M.; Kenis, P. J. A. Electroreduction of Carbon Dioxide to Hydrocarbons Using Bimetallic Cu-Pd Catalysts with Different Mixing Patterns. *J. Am. Chem. Soc.* **2017,** 139, 47-50.
33. Bertheussen, E.; Verdaguer-Casadevall, A.; Ravasio, D.; Montoya, J. H.; Trimarco, D. B.; Roy, C.; Meier, S.; Wendland, J.; Norskov, J. K.; Stephens, I. E. L.; Chorkendorff, I. Acetaldehyde as an Intermediate in the Electroreduction of Carbon Monoxide to Ethanol on Oxide-Derived Copper. *Angew. Chem., Int. Ed.* **2016,** 55, 1450-1454.
34. Hori, Y.; Takahashi, R.; Yoshinami, Y.; Murata, A. Electrochemical Reduction of CO at a Copper Electrode. *J. Phys. Chem. B* **1997,** 101, 7075-7081.
35. Feng, X. F.; Jiang, K. L.; Fan, S. S.; Kanan, M. W. A Direct Grain-Boundary-Activity Correlation for CO Electroreduction on Cu Nanoparticles. *ACS Cent. Sci.* **2016,** 2, 169-174.
36. Rosen, J.; Hutchings, G. S.; Lu, Q.; Rivera, S.; Zhou, Y.; Vlachos, D. G.; Jiao, F. Mechanistic Insights into the Electrochemical Reduction of CO2 to CO on Nanostructured Ag Surfaces. *ACS Catal.* **2015,** 5, 4293-4299.
37. Zhang, X.; Wu, Z. S.; Zhang, X.; Li, L. W.; Li, Y. Y.; Xu, H. M.; Li, X. X.; Yu, X. L.; Zhang, Z. S.; Liang, Y. Y.; Wang, H. L. Highly Selective and Active CO2 Reduction Electro-Catalysts Based on Cobalt Phthalocyanine/Carbon Nanotube Hybrid Structures. *Nat. Commun.* **2017,** 8, 14675.
38. De Luna, P.; Quintero-Bermudez, R.; Dinh, C. T.; Ross, M. B.; Bushuyev, O. S.; Todorovic, P.; Regier, T.; Kelley, S. O.; Yang, P. D.; Sargent, E. H. Catalyst Electro-Redeposition Controls Morphology and Oxidation State for Selective Carbon Dioxide Reduction. *Nat. Catal.* **2018,** 1, 103-110.
39. Kuhl, K. P.; Cave, E. R.; Abram, D. N.; Jaramillo, T. F. New Insights into the Electrochemical Reduction of Carbon Dioxide on Metallic Copper Surfaces. *Energy Environ. Sci.* **2012,** 5, 7050-7059.
40. Huang, Y.; Handoko, A. D.; Hirunsit, P.; Yeo, B. S. Electrochemical Reduction of CO2 Using Copper Single-Crystal Surfaces: Effects of CO* Coverage on the Selective Formation of Ethylene. *ACS Catal.* **2017,** 7, 1749-1756.
41. Raciti, D.; Cao, L.; Liv, K. J. T.; Rottmann, P. F.; Tang, X.; Li, C. Y.; Hicks, Z.; Bowen, K. H.; Hemker, K. J.; Mueller, T.; Wang, C. Low-Overpotential Electroreduction of Carbon Monoxide Using Copper Nanowires. *ACS Catal.* **2017,** 7, 4467-4472.
42. Chen, Y. H.; Li, C. W.; Kanan, M. W. Aqueous CO2 Reduction at Very Low Overpotential on Oxide-Derived Au Nanoparticles. *J. Am. Chem. Soc.* **2012,** 134, 19969-19972.
43. Dunwell, M.; Luc, W.; Yan, Y. S.; Jiao, F.; Xu, B. J. Understanding Surface-Mediated Electrochemical Reactions: CO2 Reduction and Beyond. *ACS Catal.* **2018,** 8, 8121-8129.
44. Schreier, M.; Yoon, Y.; Jackson, M. N.; Surendranath, Y. Competition between H and CO for Active Sites Governs Copper-Mediated Electrosynthesis of Hydrocarbon Fuels. *Angew. Chem., Int. Ed.* **2018,** 57, 10221-10225.
45. Schouten, K. J. P.; Gallent, E. P.; Koper, M. T. M. The Influence of pH on the Reduction of CO and CO2 to Hydrocarbons on Copper Electrodes. *J. Electroanal. Chem.* **2014,** 716, 53-57.
46. Montoya, J. H.; Shi, C.; Chan, K.; Norskov, J. K. Theoretical Insights into a CO Dimerization Mechanism in CO2 Electroreduction. *J. Phys. Chem. Lett.* **2015,** 6, 2032-2037.
47. Xiao, H.; Cheng, T.; Goddard, W. A.; Sundararaman, R. Mechanistic Explanation of the pH Dependence and Onset Potentials for Hydrocarbon Products from Electrochemical Reduction of CO on Cu (111). *J. Am. Chem. Soc.* **2016,** 138, 483-486.

48. Cheng, T.; Xiao, H.; Goddard, W. A. Full Atomistic Reaction Mechanism with Kinetics for CO Reduction on Cu(100) from Ab Initio Molecular Dynamics Free-Energy Calculations at 298 K. *Proc. Natl. Acad. Sci. U. S. A.* **2017,** 114, 1795-1800.
49. Goodpaster, J. D.; Bell, A. T.; Head-Gordon, M. Identification of Possible Pathways for C-C Bond Formation During Electrochemical Reduction of CO2: New Theoretical Insights from an Improved Electrochemical Model. *J. Phys. Chem. Lett.* **2016,** 7, 1471-1477.
50. Garza, A. J.; Bell, A. T.; Head-Gordon, M. Mechanism of CO2 Reduction at Copper Surfaces: Pathways to C2 Products. *ACS Catal.* **2018,** 8, 1490-1499.
51. Schouten, K. J. P.; Gallent, E. P.; Koper, M. T. M. Structure Sensitivity of the Electrochemical Reduction of Carbon Monoxide on Copper Single Crystals. *ACS Catal.* **2013,** 3, 1292-1295.
52. Wang, L.; Nitopi, S. A.; Bertheussen, E.; Orazov, M.; Morales-Guio, C. G.; Liu, X. Y.; Higgins, D. C.; Chan, K. R.; Norskov, J. K.; Hahn, C.; Jaramillo, T. F. Electrochemical Carbon Monoxide Reduction on Polycrystalline Copper: Effects of Potential, Pressure, and pH on Selectivity toward Multicarbon and Oxygenated Products. *ACS Catal.* **2018,** 8, 7445-7454.
53. Liu, X. Y.; Schlexer, P.; Xiao, J. P.; Ji, Y. F.; Wang, L.; Sandberg, R. B.; Tang, M.; Brown, K. S.; Peng, H. J.; Ringe, S.; Hahn, C.; Jaramillo, T. F.; Norskov, J. K.; Chan, K. R. pH Effects on the Electrochemical Reduction of CO(2) Towards C2 Products on Stepped Copper. *Nat. Commun.* **2019,** 10, 32.
54. Siegenthaler, H.; Juttner, K. Voltammetric Investigation of Lead Adsorption on Cu(111) Single-Crystal Substrates. *J. Electroanal. Chem.* **1984,** 163, 327-343.
55. Nasirpouri, F. On the Electrodeposition Mechanism of Pb on Copper Substrate from a Perchlorate Solution Studied by Electrochemical Quartz Crystal Microbalance. *Ionics* **2011,** 17, 331-337.
56. Baturina, O. A.; Lu, Q.; Padilla, M. A.; Xin, L.; Li, W. Z.; Serov, A.; Artyushkova, K.; Atanassov, P.; Xu, F.; Epshteyn, A.; Brintlinger, T.; Schuette, M.; Collins, G. E. CO2 Electroreduction to Hydrocarbons on Carbon-Supported Cu Nanoparticles. *ACS Catal.* **2014,** 4, 3682-3695.

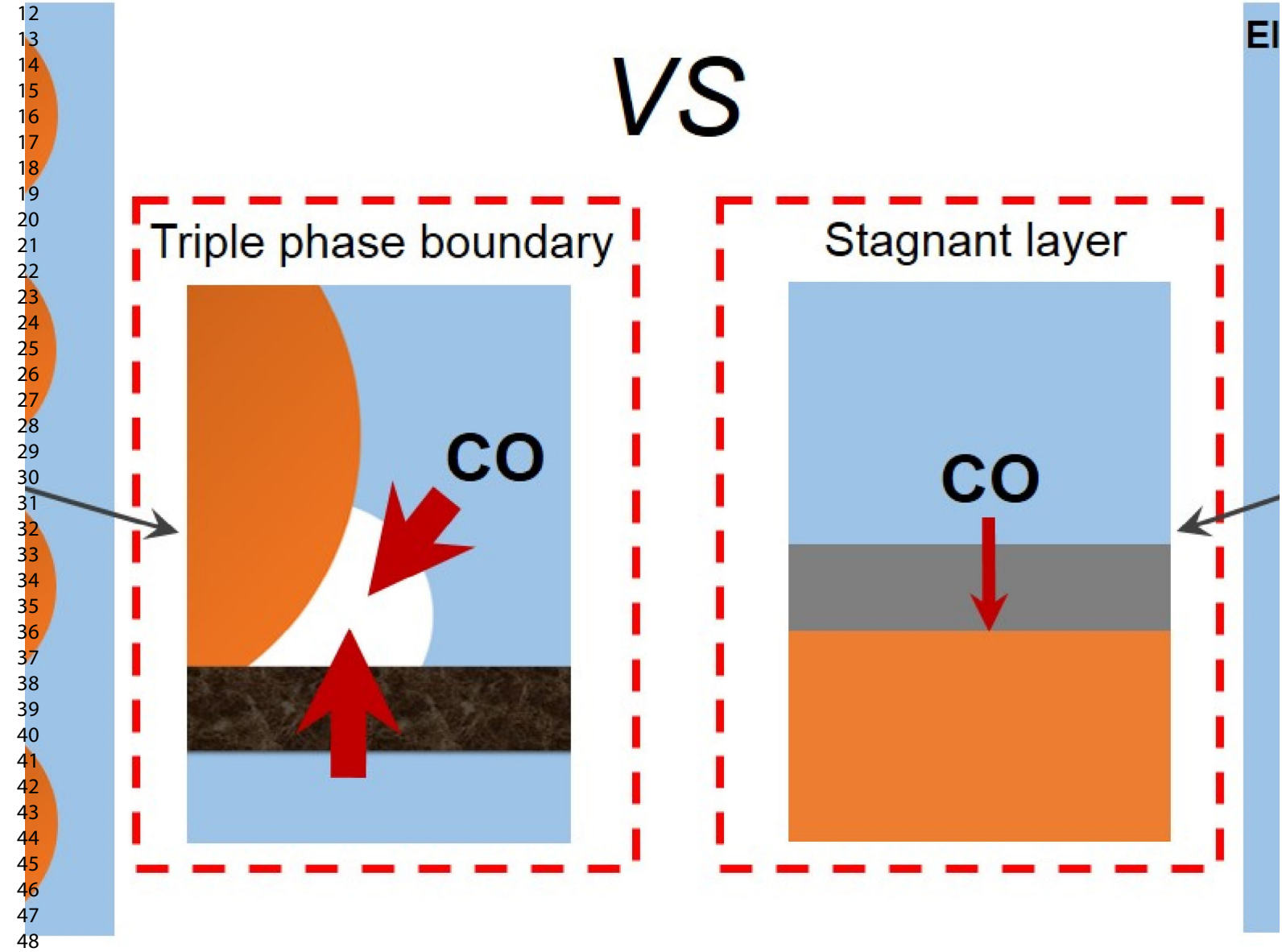
VS
Triple phase boundary
CO
Stagnant layer
CO